6-4-2015

Field line distribution of mass density at geostationary orbit

Richard Denton
Dartmouth College

Kazue Takahashi
Johns Hopkins University

Jimyoung Lee
Dartmouth College

C.K. Zeitler
Dartmouth College

N.T. Wimer
Dartmouth College

See next page for additional authors

Field Line Distribution of Mass Density at Geostationary Orbit

R. E. Denton[1], Kazue Takahashi[2], Jimyoung Lee[1], C. K. Zeitler[1,3], N. T. Wimer[1,4], L. E. Litscher[1], H. J. Singer[5], and Kyungguk Min[6]

R. E. Denton and Jinmyoung Lee, Department of Physics and Astronomy, Dartmouth College, Hanover, NH 03755, USA. (richard.e.denton@dartmouth.edu, jinmyoung.lee.16@dartmouth.edu, lauren.e.litscher.12@alum.dartmouth.org)

Kyungguk Min, 206 Allison Lab, Auburn University, Auburn, AL 36849, USA. (kmin@auburn.edu)

H. J. Singer, NOAA Space Weather Prediction Center, 325 Broadway, Boulder, CO, 80305, USA. (howard.singer@noaa.gov)

K. Takahashi, Johns Hopkins University Applied Physics Laboratory, 11100 Johns Hopkins Rd, Laurel , MD 20723-6099, USA. (kazue.takahashi@jhuapl.edu)

N. T. Wimer, Department of Mechanical Engineering, University of Colorado, Boulder, CO, 80305, USA. (nicholas.wimer@gmail.com)

C. K. Zeitler, Department of Physics, University of Illinois, 1110 West Green Street, Urbana, IL 61801-3080, USA. (Christopher.K.Zeitler.12@alum.dartmouth.org)

[1]Department of Physics and Astronomy,

Abstract. The distribution of mass density along the field lines affects the ratios of toroidal (azimuthally oscillating) Alfvén frequencies, and given the ratios of these frequencies we can get information about that distribution. Here we assume the commonly used power law form for the field line distribution, $\rho_{\rm m} = \rho_{m,eq}(LR_{\rm E}/R)^{\alpha}$, where $\rho_{m,eq}$ is the value of the mass density $\rho_{\rm m}$ at the magnetic equator, L is the L shell, $R_{\rm E}$ is the Earth's radius, R is the geocentric distance to a point on the field line, and α is the

[1]Dartmouth College, Hanover, New Hampshire, USA

[2]Applied Physics Laboratory, Johns Hopkins University, Laurel, Maryland, USA

[3]Department of Physics, University of Illinois, Urbana, Illinois, USA

[4]Department of Mechanical Engineering, University of Colorado, Boulder, Colorado, USA

[5]National Oceanic and Atmospheric Administration Space Weather Prediction Center, Boulder, Colorado, USA

[6]Department of Physics, Auburn University, Auburn, Alabama, USA

power law coefficient. Positive values of α indicate that ρ_{m} increases away from the magnetic equator, zero value indicates that ρ_{m} is constant along the magnetic field line, and negative α indicates that there is a local peak in ρ_{m} at the magnetic equator. Using 12 years of observations of toroidal Alfvén frequencies by the Geostationary Operational Environmental Satellites (GOES), we study the typical dependence of inferred values of α on the magnetic local time (MLT), the phase of the solar cycle as specified by the F10.7 extreme ultraviolet solar flux, and geomagnetic activity as specified by the auroral electrojet (AE) index. Over the mostly dayside range of the observations, we find that α decreases with respect to increasing MLT and F10.7, but increases with respect to increasing AE. We develop a formula that depends on all three parameters, $\alpha_{\mathrm{3Dmodel}} = 2.2 + 1.3 \cdot \cos\left(\mathrm{MLT} \cdot 15^{\circ}\right) + 0.0026 \cdot \mathrm{AE} \cdot \cos\left((\mathrm{MLT} - 0.8) \cdot 15^{\circ}\right) + 2.1 \cdot 10^{-5} \cdot \mathrm{AE} \cdot \mathrm{F10.7} - 0.010 \cdot \mathrm{F10.7}$, that models the binned values of α within a standard deviation of 0.3. While we do not yet have a complete theoretical understanding of why α should depend on these parameters in such a way, we do make some observations and speculations about the causes. At least part of the dependence is related to that of $\rho_{m,eq}$; higher α, corresponding to steeper variation with respect to MLAT, occurs when $\rho_{m,eq}$ is lower.

1. Introduction

The field line distribution of mass density should have an important effect on many MHD scale phenomenon. It controls the field line structure of Alfvén waves, which can make a large difference in the radial diffusion of radiation belt electrons [*Perry et al.*, 2005]. It would definitely alter the degree of focusing of fast mode waves propagating into the magnetosphere [*Kress et al.*, 2007], and will probably affect the structure of cavity mode resonances [*Kwon et al.*, 2012, and references therein].

The field line distribution of mass density also affects the frequency of toroidal (azimuthally oscillating) Alfvén waves. If the frequency of these waves, measured by ground magnetometers [*Waters et al.*, 2006] or spacecraft [*Denton*, 2006], is used to calculate the magnetospheric mass density, an incorrect assumption about the field line distribution can cause an error in the inferred mass density. Since the theoretical frequency of Alfvén waves $f_{\rm th}$ will be proportional to the equatorial Alfvén speed $\propto 1/\sqrt{\rho_{\rm m}}$, the equatorial mass density $\rho_{\rm m}$ can be found from $f_{\rm obs}/f_{\rm th}(1\,{\rm amu/cm^3}) = \sqrt{(1\,{\rm amu/cm^3})/\rho_{\rm m}}$, where $f_{\rm obs}$ is the observed Alfvén frequency, and $f_{\rm th}(1\,{\rm amu/cm^3})$ is the theoretical frequency for an equatorial mass density of 1 amu/cm^3. This means that there will be an error in the inferred $\rho_{\rm m}$ proportional to the error of $f_{\rm th}^2$.

The magnitude of such errors can be estimated from the normalized Alfvén frequencies calculated by *Schulz* [1996] if we assume the power law field line distribution for $\rho_{\rm m}$

$$\rho_{\rm m} = \rho_{m,eq}\left(\frac{LR_{\rm E}}{R}\right)^{\alpha}, \tag{1}$$

that has been used by many researchers [*Waters et al.*, 2006; *Denton*, 2006]. Here $\rho_{m,eq}$ is the value of the mass density $\rho_{\rm m}$ at the magnetic equator; $L \equiv R_{\rm max}/R_{\rm E}$, where $R_{\rm max}$ is the

maximum geocentric distance to any point on the field line, and R_E is the Earth's radius; and α is the power law coefficient (Schulz's m). For the purpose of defining L we use the TS05 magnetic field model [*Tsyganenko and Sitnov*, 2005]. Note that $\alpha = 0$ corresponds to constant ρ_m along the field line, $\alpha > 0$ corresponds to ρ_m that increases with respect to the magnetic latitude, MLAT, toward the ionosphere, and $\alpha < 0$ corresponds to ρ_m that is locally peaked at the magnetic equator. If one includes the part of the field line that approaches the ionosphere, $\alpha > 0$ would seem to be most realistic, but it is the portion of the magnetic field line close to the magnetic equator (where the magnetic field B is small) that often plays a dominant role in determining the Alfvén frequency. So it is possible for $\alpha < 0$ to be relevant, indicating that ρ_m is locally peaked near the magnetic equator, even though ρ_m must eventually increase at large MLAT. In previous calculations using data from the Geostationary Operational Environmental Satellites (GOES), the field line distribution implied by (1) was probably not accurate for |MLAT| beyond about 25°[*Takahashi and Denton*, 2007].

If we use the fundamental mode frequency at geostationary orbit to infer ρ_m and assume that α is equal to 3, but the realistic field line distribution corresponds to $\alpha = 0$, the inferred value of ρ_m will be 15% lower than the actual value. For the purpose of calculating the mass density, it would be useful to reduce even this uncertainty. But the uncertainty increases if a harmonic higher than the fundamental mode is used. If we use the third harmonic to infer ρ_m, the estimated ρ_m becomes 33% lower than the actual value. This error would increase if the mass density is locally peaked at the magnetic equator ($\alpha < 0$). The third harmonic is the most frequently observed toroidal Alfvén wave observed by GOES [*Takahashi et al.*, 2010], so this is an important case.

The field line distribution of $\rho_{\rm m}$ can be estimated based on the ratios of frequencies of the harmonics of toroidal Alfvén waves [*Takahashi and McPherron*, 1982; *Price et al.*, 1999; *Takahashi and Denton*, 2007; *Denton et al.*, 2006b, 2009]. The basic idea is fairly simple. Mass density localized on one part of the field line affects the frequencies of different harmonics to a different extent. For instance, a peak in $\rho_{\rm m}$ strongly localized to the magnetic equator would lower the frequency of the fundamental mode ($n = 1$) and other odd harmonics, because those modes have a nonzero velocity at the magnetic equator. But such a steep peak in $\rho_{\rm m}$ would not lower the frequency of the second harmonic ($n = 2$) or other even harmonics, because the velocity is zero for those modes at the magnetic equator. The inertia only affects the mode if there is acceleration at the position of that inertia. Consequently, if a steep peak in $\rho_{\rm m}$ is added at the magnetic equator, the ratio f_2/f_1 will increase. In this paper, the frequency ratios will be normalized to the most frequently observed third harmonic, so that our normalized frequencies $\overline{f}_n \equiv f_n/f_3$. By varying α so as to reduce the least squared difference between the observed and theoretical values of $\overline{f}_n$, we infer the most appropriate value of α.

In principle, if one wants to use toroidal Alfvén frequencies to get $\rho_{\rm m}$ for a particular event, one might be able to measure the frequencies of several harmonics and get both $\rho_{m,eq}$ and α. *Denton et al.* [2009] have apparently done this successfully using the frequencies of toroidal Alfvén waves measured by the Cluster spacecraft. But in most cases, the error in inferred values of α found for particular events is large [*Takahashi and McPherron*, 1982; *Denton et al.*, 2001, 2004] owing to the sensitivity of the toroidal Alfvén frequencies to the field line distribution [*Denton and Gallagher*, 2000]. For that reason, most of our recent studies of the field line distribution of $\rho_{\rm m}$ have been statistical [*Takahashi et al.*,

2004; *Denton et al.*, 2006b; *Takahashi and Denton*, 2007]. Using many observations of the normalized frequency ratios $\overline{f}_n$, we can get an accurate measure of at least the typical field line distribution.

Angerami and Carpenter [1966] presented theoretical field line distributions that can be approximated by values of α between 0.5 and 1 for diffusive equilibrium (more likely relevant in the high density plasmasphere [*Takahashi et al.*, 2014, and references therein]) and $\alpha = 4$ for a collisionless equilibrium (possibly relevant for the low density plasmatrough) [*Takahashi et al.*, 2004]. *Denton et al.* [2006b] did a statistical study of toroidal Alfvén frequencies measured by the Combined Release and Radiation Effects Satellite (CRRES), and recommended $\alpha = 1$ for the field line distribution at $L > 5$ if the power law model was used. This includes times during which the spacecraft might have been in the plasmasphere or plasmatrough. They found evidence for a local peak in ρ_{m} at the magnetic equator under certain conditions, especially with large geomagnetic activity (large Kp index or large negative Dst). *Takahashi and Denton* [2007], did a statistical study using toroidal Alfvén frequencies measured by GOES and found that there was evidence for a local peak in ρ_{m} at the magnetic equator in the afternoon magnetic local time MLT sector, but not in the dawn MLT sector. Studies finding α at lower values of L have been summarized by *Denton* [2006].

Here our goal is to develop a model for α that depends on MLT, geomagnetic activity as indicated by the auroral electrojet (AE) index, and solar radiation as indicated by the F10.7 index. The value of AE may be related to substorm activity. The value of F10.7 is related to the phase of the solar cycle. Large F10.7 corresponds to solar maximum, while small F10.7 corresponds to solar minimum. In section 2, we describe the data and

method used in the study; in section 3, we describe our modeling results for variation with respect to a single parameter (MLT, F10.7, or AE); in section 4, we describe our modeling results with simultaneous variation of all three parameters; and in section 5 we discuss these results.

2. Data and Method

The database of toroidal (azimuthally oscillating) Alfvén wave frequencies that we will use has been described by *Takahashi et al.* [2010]. Frequencies were obtained from magnetometer data on five Geostationary Operational Environmental Satellites (GOES) over a 12 year period from 1980 to 1991. The data was scanned in 30 min time windows that moved forward in 10 min steps. The maximum entropy method (MEM) [*Press et al.*, 1986] was used to find peaks in the power spectra, and an interactive method was used to identify most of the third harmonic ($n = 3$) frequencies. Using the algorithm below, some additional third harmonic frequencies were identified automatically because their frequencies and times of observation were close to those of manually identified third harmonic frequencies.

Whereas *Takahashi et al.* [2010] used only the most commonly observed third harmonic ($n = 3$), we will make use of harmonics up to $n = 4$. In order to determine the harmonic number, we normalize all the frequencies to third harmonic frequencies. In order to normalize a frequency observed at time t, a third harmonic frequency had to be identified within 10 min of t. Considering the 10 min resolution of our data, this means that a third harmonic frequency had to be identified either at the time of observation or one time step earlier or later. If a third harmonic frequency was identified on one side of an observation and another third harmonic frequency was identified within 20 min on the

other side of the observation, we interpolated the two third harmonic frequencies to the time of observation. With the observed frequency f and the nearby or interpolated third harmonic frequency f_3, we calculate the normalized frequency $\bar{f} \equiv f/f_3$.

Since we are normalizing to the third harmonic frequencies, we discarded the normalized third harmonic frequencies (equal to unity). We further limited the data in several ways. We discarded normalized frequencies above 1.5; these values occur for harmonics over $n = 4$. For each harmonic number n, we calculated the uncertainty of the normalized frequency $\delta\bar{f}_n$, using

$$\delta\bar{f}_n = \bar{f}_n \sqrt{\left(\frac{\delta f_n}{f_n}\right)^2 + \left(\frac{\delta f_3}{f_3}\right)^2}, \tag{2}$$

and discarded the resulting normalized frequencies for which the uncertainty was greater than 0.1. And we further limited the data to time periods for which the AE index was available. This eliminated most of the one and a half year period between the midpoint of 1988 and the beginning of 1990. While the frequency ratios of the Alfvén waves varied with geomagnetic activity based on the Kp index, the Dst index, and the AE index, we found that there was a somewhat greater dependence on AE than on the other indices (not shown). Therefore we decided to use the AE index as a measure of geomagnetic activity. After these reductions, we still had 211,808 normalized frequencies.

Figure 1 shows the distribution of normalized frequencies $\bar{f}$ used in our study. With these frequencies, we will examine the statistical variation of the field line distribution. Here, we solve for Alfvén wave eigenmodes using the procedure of *Denton et al.* [2006b]. We use the *Singer et al.* [1981] wave equation with the power law form (1) for the field line distribution of mass density and with a dipole magnetic field at $L = 6.8$, a nominal equatorial distance for GOES spacecraft. For the entire set of times of our frequency

measurements, the mean L value was 6.8 with a standard deviation of 0.13. Note that *Takahashi et al.* [2004] found, for the purpose of determining the field line distribution, that the use of a different magnetic field model did not significantly alter the results. We assume that there is a perfectly conducting boundary at an altitude of 100 km. Then we start with a guess for the power law coefficient α and vary α and $\rho_{m,eq}$ (at each value of α) to find the best fit between the observed and calculated frequency ratios $\bar{f}$ by minimizing the quantity

$$S \equiv \sum_{n=1...4} w_n \left(\bar{f}_{\mathrm{obs},n} - f_{\mathrm{th},n}\right)^2, \tag{3}$$

where for each harmonic n, the weight $w_n = 1/(\delta\bar{f}_{\mathrm{obs},n})^2$, $\delta\bar{f}_{\mathrm{obs},n}$ is the uncertainty in the observed normalized frequency $\bar{f}_{\mathrm{obs},n}$, and $f_{\mathrm{th},n}$ is the theoretical frequency. While $\bar{f}_{\mathrm{obs},3}$ is unity, $f_{\mathrm{th},3}$ is an unnormalized frequency (dependent on $\rho_{m,eq}$), and is only approximately equal to unity (because of the minimization with respect to $\rho_{m,eq}$). The solution leads to best fit values for both $\rho_{\mathrm{m,eq}}$ and α, but the value of $\rho_{m,eq}$ is meaningless because the observed frequencies were rescaled (normalized to $f_{\mathrm{obs},n}$). Note that variation in $\rho_{\mathrm{m,eq}}$ merely changes all the frequencies $f_{\mathrm{th},n}$ by a common factor. Here we are only interested in the values of α.

For $n = 3$, we used the weight $w_3 = \sum_{n=1,2,4}(\bar{f}_{\mathrm{obs},n}/\delta\bar{f}_{\mathrm{obs},n})^2$. This formula is motivated by the idea that we could work backwards to get the third harmonic frequency from the other harmonics. We assume that the uncertainty for f_3 based on another harmonic is equal to the relative error of that harmonic. The absolute error would be unity times that relative error, and the separate weights add in quadrature assuming that they are independent measurements [*Lyons*, 1991]. We tested this method with sets of data including random errors and it yielded a more accurate and precise result than the other methods

we tried (including normalizing the theoretical frequencies to $f_{\mathrm{th},3}$ and fitting $\bar{f}_{\mathrm{obs},n}$ to $\bar{f}_{\mathrm{th},n}$ for only $n = 1$, 2, and 4).

For instance, fitting Gaussians to the three peaks in Figure 1, we find $\bar{f}_1 \equiv f_1/f_3 = 0.236 \pm 0.034$, $\bar{f}_2 = 0.638 \pm 0.037$, and $\bar{f}_4 = 1.360 \pm 0.073$, where the number after "±" is the standard deviation of the Gaussian fit. Using the peak frequencies of the three peaks, we find $\alpha = 1.1$, a reasonable value based on previous studies [*Denton*, 2006; *Denton et al.*, 2006b]. This value indicates that the mass density increases mildly as one moves from the magnetic equator (where LR_{E}/R in (1) equals unity) to higher magnetic latitude, MLAT (where the geocentric radius $R < LR_{\mathrm{E}}$).

In order to get a measure of the possible spread in α based on the spread (standard deviation) of the observed frequency ratios, we do a Monte Carlo set of calculations with a random set of frequencies generated using probabilities consistent with the standard deviations of the frequencies. In other words, a large number of random choices would give for each peak a Gaussian distribution of frequencies with the same standard deviation. Using 1000 random combinations of the three frequencies, we find a median value of α of 1.2, with the first quartile and third quartile values of -1.7 and 3.0, respectively. That is, one fourth of the 1000 α values were below -1.7, and one fourth were above 3.0. The mean and standard deviation values are 0.3 and 3.6, respectively. Note that the mean values are typically skewed toward negative values from the value based on the peak frequencies. This is because a Gaussian in the linear (rather than log) frequency is used, and negative changes in frequency have a larger effect on the results because they lead to a larger logarithmic or factor change in the frequency. The fundamental mode ($n = 1$), with small frequency, is especially sensitive to this effect, and decreased fundamental mode frequency

is correlated with peaked mass density at the magnetic equator, corresponding to negative α.

Based on these numbers (standard deviation of 3.6), one might think that the value of α is known very imprecisely. There are, however, two considerations that reduce the strength of this conclusion. First of all, we are primarily interested in determining the most common or typical field line distribution. The standard deviation of a mean is reduced relative to the standard deviation of a set of measurements roughly by the square root of the number of measurements. Using the number of frequencies measured in the 4th harmonic ($n = 4$, with the smallest number of measurements), equal to 58,400, we estimate the standard deviation of the mean in α as $3.6/\sqrt{58400} = 0.015$, a very small number.

But, as discussed by *Takahashi and Denton* [2007], there is reason to suspect that the spread in α values corresponding to the real field line distribution of the magnetospheric mass density at geostationary orbit is smaller than the spread of 3.6 consistent with the observations. This is because the uncertainty in frequency ratio due to the uncertainty of individual frequency measurements makes up a significant fraction of the total spread in the frequency ratios. Thus the real spread in the precise frequency ratios and the corresponding spread in α values are likely to be smaller.

For instance, assuming a resolution of 0.56 mHz due to a 30 min time window, we use (2) to calculate the root mean squared error $\delta\bar{f}_n$ for the three harmonics $n = 1$, 2, and 4, and get 0.027, 0.026, and 0.043, respectively. Comparing to the standard deviation of the Gaussian fits, 0.034, 0.037, and 0.073, we see that the relative errors due to resolution account for a significant fraction of the uncertainty, especially for $n = 1$, and

2. Assuming that the measurement uncertainty due to resolution and the real uncertainty add in quadrature (square root of the sum of the squares), we estimate a real uncertainty of 0.022, 0.027, and 0.063 for $n = 1$, 2, and 3, respectively. If we use these uncertainties for the frequency ratios, we find first quartile, median, and third quartile values of -1.0, 1.0, and 2.3, respectively, or a mean value of α of 0.4 with standard deviation of 2.5. So the standard deviation in this case (2.5) is lower than that found using the total spread in the relative frequencies (3.5).

Below we will find α in three-dimensional bins with different combinations of MLT, AE, and F10.7. The standard deviation of the values of α in those bins is 1.0. Since there are roughly an equal number of frequencies in each of these bins, the uncertainty in α for all the data due to variation in MLT, AE, and F10.7 must also be about 1.0. Assuming again that uncertainties add in quadrature, the unexplained uncertainty in α would be roughly $\sqrt{(2.5)^2 - (1.0)^2} = 2.3$.

We will not do this detailed a calculation of uncertainty for the remaining results. But a reasonable spread in α around the values we calculate is probably something like 2.3. The mean values, however, are likely to be very close to the values that we find.

3. One Dimensional Modeling

Now for each of the three variables, MLT, F10.7, and AE, we divide our set of frequencies into 8 bins. We call this 1D binning. Values of F10.7 measured in solar flux units (sfu $= 10^{-22}\mathrm{Wm}^{-2}\mathrm{Hz}^{-1}$), and AE measured in nT, as well as solar wind parameters needed for the TS05 magnetic field model, are interpolated from hourly values from the National Aeronautics and Space Administration Goddard Space Flight Center OMNI data set through OMNIWeb [*King and Papitashvili*, 2005]. MLT is measured in h. The bin

divisions are determined using quantiles Q_i that extend to i/8th of the data points, where i is an integer between 1 and 7, when those data points are ordered from lowest to highest. Thus each bin has one eighth of the frequencies. This method ensures that we have comparable statistics in each bin. Table 1 shows the quantile values for each of the three variables in addition to the minimum value (or Q_0 for 0/8th of the data) and maximum value (or Q_8 for 8/8th of the data). The boldface even numbered quantile values, which are quartiles, will be used in section 4 to divide the data into four bins.

Now for each of the three variables, and within each of the 8 bins, we fit Gaussians to the $\bar{f}_1$, $\bar{f}_2$, and $\bar{f}_4$ peaks. The distribution of frequencies and Gaussian fits are shown in Figure 2 for the first bin of MLT with 0.01 h $\leq$ MLT $<$ 5.39 h. The data used for the Gaussian fits includes bins with a number of frequencies equal to at least half the peak value (black x symbols in Figure 2). Because some peaks were steep (especially for the 3D binning described in section 4), we added for each peak two additional points with exactly one half the peak value (black circles in Figure 2). These were obtained by interpolation using the values in adjacent bins. Then the best least-squares Gaussian fits were obtained for each peak (red curves in Figure 2). The data used for the fitting was limited to one half the peak value in order to avoid contamination by adjacent peaks (particularly for $n = 4$). The rest of the frequency distribution, while not used for the fits, is shown in Figure 2 as the dotted black curve.

Figure 3 shows the peak normalized frequency $\bar{f}_n$ (black x symbols) for $n = 1$ (row A), $n = 2$ (row B), and $n = 4$ (row C) for the binned distributions of MLT (column a), F10.7 (column b), and AE (column c). The fact that there is variation in the frequency ratios with respect to MLT, F10.7, and AE, indicates that the field line distribution is

varying with respect to these parameters. Because there is some apparent noisiness in the values, we smooth the data. The values binned by F10.7 and AE are fit with a quadratic polynomial. We didn't feel that the polynomial fits with respect to MLT were as satisfactory, so in that case we smoothed the interior binned values y_i for bin i using $0.5y_i + 0.25(y_{i-1} + y_{i+1})$. The smoothed values are shown by the red curves in Figure 3. The standard deviation of the observed frequencies is shown by the error bars in Figure 3, and the spread of observed frequencies in the peaks (length of error bars) is larger than the variation of the peak frequencies (x symbols) with respect to the parameters on the horizontal axis of each panel. As was discussed in section 2, some of this spread is probably from the uncertainty due to the resolution in frequency. But even if this is factored out, the spread in observed frequencies is larger than the variation with respect to MLT, F10.7, or AE.

For each 1D bin, the wave equation is solved to find the value of α for which the theoretical frequencies best match the smoothed frequency ratios from Figure 3. The black open circles in Figure 4 show the results for variation with respect to MLT (Figure 4a), F10.7 (Figure 4b), and AE (Figure 4c). From this plot, we see that α decreases with respect to MLT (over the dayside range of MLT sampled) and F10.7, but increases with respect to AE. The strongest dependence is on MLT.

Using the Eureqa Formulize nonlinear genetic regression software [*Schmidt and Lipson*, 2009] to find potential mathematical models for the F10.7 and AE dependence, and using a Fourier expansion for the MLT dependence up to the sine and cosine of twice the angle around the Earth, we chose the following analytical formulas:

$$\alpha_{\mathrm{1Dmodel,MLT}} = 1.1 + 1.4\cos((\mathrm{MLT} - 2.1)\cdot 15^\circ) + 0.3\cos(2\cdot(\mathrm{MLT} - 2.8)\cdot 15^\circ), \quad (4)$$

$$\alpha_{\mathrm{1Dmodel,F10.7}} = 2.3 - \frac{49}{\mathrm{F10.7}} - 0.0065 \cdot \mathrm{F10.7}, \quad (5)$$

$$\alpha_{\mathrm{1Dmodel,AE}} = 0.8 + 0.00116\mathrm{AE}. \quad (6)$$

These analytical formulas were chosen because they well fit the data points, are relatively simple, and are relatively well behaved over the full range of parameter values (from minimum to maximum) listed in Table 1. The weighted standard deviation of these formulas from the data points is less than 0.05 for each model, where the weights were the squared inverse of third quartile value of α minus the first quartile value for a distribution of 1000 frequencies consistent with the observed spread in frequencies. The red curves in Figure 4 show these formulas over these full ranges, (4) in Figure 4a, (5) in Figure 4b, and (6) in Figure 4c. Note that (4) in Figure 4a is periodic, and (5) in Figure 4b and (6) in Figure 4c vary linearly with respect to F10.7 and AE, respectively, at large values.

Based on the behavior of the data points, these were conservative choices and they lead to reasonable curves where extrapolated. One should, however, use caution when extrapolating. When far away from the range of data points in Figure 4, 4.2 h $\leq$ MLT $\leq$ 16.2 h, F10.7 $\leq$ 218 sfu, and AE $\leq$ 603 nT, the formulas are without doubt questionable.

Again, a Monte Carlo simulation using the observed spread in frequencies leads to a large variation in the inferred α at the data points; the standard deviations for the points range between 3.3 and 4.2.

4. Three Dimensional Modeling

Now we want to divide the frequency data using simultaneous divisions with respect to all three parameters, MLT, F10.7, and AE. We call this 3D binning. In order to have adequate statistics in each bin, we use 4 bins for each variable, so that the total number

of bins is $4^3 = 64$. The boundaries for the bins for each parameter are the quartile values for each individual parameter. These are the bold values listed in Table 1. The mean values of each parameter in each of the four bins with respect to an individual parameter are listed in Table 2. Note that the mean values are between the quartile values listed in Table 1, as they must be. But the mean values are not necessarily near the center of each possible range. For instance, the mean MLT value in the first of four bins (5.1 h from Table 2) is close to the upper range of the first bin (6.69 h from Table 1), though this bin includes values ranging from 0.01 h to 6.69 h (Table 1). Similarly the mean in the 4th MLT bin (14.6 h) is close to the lower boundary of the 4th bin (11.9 h). This is because the distribution of toroidal Alfven waves is strongly peaked on the dayside [*Takahashi et al.*, 2010]. Because of this, our mean bin values will be concentrated also on the dayside (ranging from MLT = 5.1 h to 14.6 h).

Note also that the number of frequencies in each 3D bin will not be exactly equal, as they were for the 1D bins, because the quartile values are chosen for each parameter using all the data. But the number of frequencies in the 3D bins typically vary by only about a factor of 2.

Figure 5 shows the distribution of frequencies for the 3D bin with the lowest values of MLT, F10.7, and AE in the same format as Figure 2. The ranges of the parameters for this bin extend up to the lowest bold numbers listed in Table 1 and are also indicated in the figure. The red curves in the figure show the Gaussian fits to the peaks. The frequency distribution is definitely more noisy here than was the case of Figure 2. This is because the 3D bins contain roughly 1/64 of the data, whereas the 1D bins contained 1/8

of the data. Nevertheless, we consider the data adequate to find the three peaks. And we verified that all 64 sets of peaks were of similar quality.

The Alfvén wave equation is solved for each of the 64 sets of frequency ratios corresponding to the 64 3D bins. The values of α based on the peak frequencies for each bin vary between -1.1 and 2.9. For each set of ratios, we vary α until the calculated frequency ratios best matches the binned ratios in a least-squares sense. Then using linear regression with some guidance from Eureqa Formulize, we find the following model for the 3D α values as a function of MLT, F10.7, and AE.

$$\begin{aligned} \alpha_{\mathrm{3Dmodel}} \;=\; & 2.2 + 1.3 \cdot \cos\left(\mathrm{MLT} \cdot 15^\circ\right) \\ & +0.0026 \cdot \mathrm{AE} \cdot \cos\left((\mathrm{MLT} - 0.8) \cdot 15^\circ\right) \\ & +2.1 \cdot 10^{-5} \cdot \mathrm{AE} \cdot \mathrm{F10.7} - 0.010 \cdot \mathrm{F10.7}, \end{aligned} \tag{7}$$

where MLT is in h, AE is in nT, and F10.7 is in sfu. To get this formula, we minimize the weighted standard deviation in the α values calculated using the peak frequencies, using weights equal to the squared inverse of the difference in the third quartile α value and the first quartile value using 1000 random frequencies for each bin. This formula fits the 3D α values within a weighted standard deviation of 0.3. The weighted standard deviation of the data in the bins was 1.0 around a weighted average of 1.1. So (7) accounts for about 90% of the squared variation (proportional to the standard deviation squared) in the binned values.

The 3D bin values of MLT, F10.7, and AE are close to, but not exactly the same, as the values listed in Table 2. For the purpose of plotting only, we adjust the 3D α values

using the following formula

$$\alpha^{\text{adjusted}}_{i,j,k} = \alpha^{\text{original}}_{i,j,k} \quad +\alpha_{\text{3Dmodel}}\left(\text{MLT}_i, \text{F10.7}_j, \text{AE}_k\right) \\ -\alpha_{\text{3Dmodel}}\left(\text{MLT}_{i,j,k}, \text{F10.7}_{i,j,k}, \text{AE}_{i,j,k}\right) \tag{8}$$

where MLT_i, F10.7_j, and AE_k are the 1D bin values listed in Table 2, and $\text{MLT}_{i,j,k}$, $\text{F10.7}_{i,j,k}$, and $\text{AE}_{i,j,k}$ are the mean parameter values in the 3D bins for the ith MLT bin, the jth F10.7 bin, and the kth AE bin. With this adjustment, we hope to be able to see the variation in one of the three parameters keeping the other parameters constant. Most of the adjustments are small. The average adjustment is 0.02, showing that the adjustments do not significantly change the α values on average. The average absolute value of the adjustments is 0.07. The largest absolute value of the adjustment is 0.40. The largest part of this largest adjustment is due to a difference in the 3D bin value of AE from the 1D value, but the difference in MLT also contributes. In any case, all of these adjustments are relatively small compared to the variation over the 3D bins (from -1.1 to 2.9).

Figure 6 shows line plots of α^{adjusted} versus AE for the various combinations of MLT and F10.7. For the most part, α^{adjusted} decreases with respect to increasing MLT, as indicated by the fact that for most data points the α^{adjusted} values are highest for the thick solid curves and lowest for the dotted curves. There are some exceptions. For instance, the rightmost data point on the dotted red curve, corresponding to the highest values of AE, MLT, and F10.7 may be an outlier. Again, for the most part, α^{adjusted} decreases with respect to increasing F10.7, as indicated by the fact that the curves with red color tend to be the lowest, while the curves with black color tends to be the highest. The AE dependence is more complicated. At MLT = 5.1 h (thick curves), α^{adjusted} tends to

increase with respect to AE. But at the latest local times, MLT = 10.3 h and 14.6 h (dashed and dotted curves), α^{adjusted} increases with respect to AE only at large F10.7 (red curves).

These trends can be seen in (7). The cosine function with MLT as an argument peaks near MLT = 0 h, which is significantly closer to the first bin value of MLT = 5.1 h than to the last bin value of MLT = 14.6 h. Therefore, α_{3Dmodel} decreases with respect to MLT over the four MLT bin values. And α_{3Dmodel} has a negative term with F10.7, so α_{3Dmodel} generally decreases with respect to F10.7. Runs of Eureqa Formulize indicated that the most important terms with AE were terms that combined AE with MLT or F10.7 dependence. In fact, (7) does not have a simple linear term involving AE. The AE terms in α_{3Dmodel} are multiplied by a cosine function in MLT that peaks near MLT = 0 h or by F10.7. So α_{3Dmodel} increases with respect to AE mainly at MLT near 0 h or at large F10.7.

Figure 7 also shows α_{adjusted} in the 3D bins of the space of (MLT,F10.7,AE) (column a), as well as α_{model} (column b), and the difference $\alpha_{\text{model}} - \alpha_{\text{adjusted}}$ (column c). Again, α becomes more negative (indicated in Figure 7a and b by more bluish color) with respect to increasing MLT (over the dayside range of MLT values used here) and with increasing F10.7. We indicate in Figure 7 the bins for which the AE dependence makes a difference of at least 0.4 with green circles. If the AE dependence is positive, the circles are filled with red color, whereas if the AE dependence is negative, the circles are filled with blue color. (The circles around the blue color may appear cyan due to their proximity to the blue color.) The actual AE dependent terms in (7) are dominantly positive for the dayside range of MLT shown in Figure 7, but in order to show the effect of including

the AE dependence, we generated a second model without the AE dependent terms, $\alpha_{\mathrm{modelMinusAE}} \equiv 2.1 + 1.8\cos\left((\mathrm{MLT} - 0.5)\cdot 15^\circ\right) - 0.0047$ F10.7, and subtracted the value of $\alpha_{\mathrm{modelMinusAE}}$ from α_{model} calculated using (7). With this procedure, we find that $\alpha_{\mathrm{model}} - \alpha_{\mathrm{modelMinusAE}}$ is negative at small AE. The AE dependence is important for MLT close to 0 h and for large F10.7, as was described in reference to Figure 6, and these dependencies explain the pattern of green circles in Figure 7.

Finally, as suggested by the weighted standard deviations mentioned above (0.3 for the difference between model and data versus 1.0 for the data itself), Figure 7 shows that the difference $\alpha_{\mathrm{model}} - \alpha_{\mathrm{adjusted}}$ is much less than the variation in $\alpha_{\mathrm{adjusted}}$ over the 3D space, indicating that the model is doing a good job representing most of the variation of α in Figure 7. Once again, the standard deviation of the α values consistent with the observed spread in the frequencies is large, between 2.9 and 4.4 in the 64 bins. Such spreads are somewhat larger than the variation of α in the bins which is shown in Figure 7. Therefore there may be a significant variation of α values around that of α_{model}, but α_{model} should well predict the typical α values.

While (7) is a reasonable formula for most of the possible range of parameters, the terms proportional to AE and F10.7, and especially the one proportional to both, can get very large for large values of AE and F10.7. So we do not consider (7) to be a good model for the full range of possible parameters. One possible way to handle this problem would be to limit the range of $\alpha_{\mathrm{3Dmodel}}$ to values between -2 and +4. These limits are close to the limits of α in Figure 6.

5. Discussion

Early theoretical calculations by *Angerami and Carpenter* [1966] suggested that realistic values of α might range between 0.5 or 1 and 4. *Takahashi and Denton* [2007] found that α tends to be more negative at afternoon MLT values. This result is consistent with our current findings. *Denton et al.* [2006b, and references therein], using data from the CRRES spacecraft, found that α appeared to be negative, suggesting a local peak in mass density at the magnetic equator. They investigated the relation of this local peak to geomagnetic activity, using the Kp and Dst indices. We found that there is a higher correlation with AE (not shown), and have used that in our model. Whereas *Denton et al.* [2006b] found more negative α correlated with increased geomagnetic activity as indicated by Kp or negative Dst, we find more positive α correlated with increased geomagnetic activity as indicated by larger AE.

Ideally, we would now explain all the dependencies that we see. Unfortunately, we are not able to do that. But we can make some observations and speculations. The midnight to dusk plasma at geostationary orbit is often on magnetic flux tubes that drift on open $\mathbf{E} \times \mathbf{B}$ drift paths eastward from the magnetotail on the nightside to the magnetopause on the dayside. A predominantly cold or warm population called the plasma cloak gradually fills these flux tubes through upflow from the ionosphere as they travel on these trajectories [*Chappell et al.*, 2008; *Lee and Angelopoulos*, 2014]. At dawn local time, this population of particles tends to be moving up the field line (particles have a field aligned pitch angle distribution). Therefore it is certainly possible that the density of particles would be higher at high magnetic latitudes closer to the source of the population at low altitude, and thus correspond to large positive values of α. As this population drifts around the

dayside magnetosphere toward dusk, it may gradually refill at the magnetic equator and become more trapped. A highly trapped (90° pitch angle population) would be peaked at the magnetic equator so that negative α would be appropriate. Another possible reason for more negative α at dusk is that there is at that location a greater contribution to the mass density from trapped ring current particles (with 10s of keV temperature), especially O+, that drift westward (because of the westward ∇B and curvature drifts) from the magnetotail.

Negative values of α occur at large F10.7, for which we expect a larger concentration of O+ [*Denton et al.*, 2011]. Perhaps the O+ becomes more trapped than the H+ for reasons we don't currently understand. Perhaps the centrifugal force due to the rotational motion around the Earth creates a pseudo-potential that preferentially traps the O+ or perhaps the O+ is heated in the perpendicular direction by the Alfvén waves themselves [*Denton et al.*, 2006a] or by electromagnetic ion cyclotron (EMIC) or other waves. Or perhaps the detailed wave particle interactions that lead to trapping favor the trapping of high mass particles.

Greater activity as indicated by larger AE might correspond to greater upflow of new particles in the plasma cloak, so that more positive α may be appropriate. The effect of greater AE on α would be concentrated in the predawn local time sector where the plasma in the cloak starts to flow up the field lines that are $\mathbf{E} \times \mathbf{B}$ drifting eastward from the nightside.

These factors relate at least somewhat to the buildup of mass near the magnetic equator. We mentioned that equatorial refilling may occur as the local time changes from dawn to dusk [*McComas et al.*, 1993; *Menk et al.*, 1999; *Galvan et al.*, 2008] and that there might

be refilling from the ionosphere on the nightside correlated with AE. We stated that there is more O+ and therefore larger mass density at solar maximum, corresponding to larger F10.7. The question arises as to whether the α values are primarily related to the value of the equatorial mass density itself. Clearly, if the mass density is very low at the magnetic equator, it must eventually increase rapidly with respect to MLAT so as to reach ionospheric values; that is, α should be large.

In order to investigate the correlation of α with the equatorial mass density, we find the log average value of ρ_{m} in the 64 3-D bins in order to model the variation of α in these bins with ρ_{m} alone. First we solve for the equatorial mass density for each point in our data set. As mentioned in the Introduction, the inferred equatorial mass density depends on the value of α that is assumed. We used a formula for α that was very close to that of (7). (Equation (7) has been slightly modified since we calculated the mass densities due to slight modifications in our method, but the difference would have only a slight effect on the inferred equatorial mass density.) If we model ρ_{m} with the same functional form used for (7), we find

$$\begin{aligned}\log_{10}(\rho_{\mathrm{m}}) \;=\; & 0.46 - 0.17 \cdot \cos\left((\mathrm{MLT} - 3.7) \cdot 15^{\circ}\right) \\ & -0.00022 \cdot \mathrm{AE} \cdot \cos\left((\mathrm{MLT} - 23.3) \cdot 15^{\circ}\right) \\ & -1.7 \cdot 10^{-6} \cdot \mathrm{AE} \cdot \mathrm{F10.7} + 0.0042 \cdot \mathrm{F10.7} \end{aligned} \tag{9}$$

with a weighted standard deviation of 0.19 (a factor of 1.5). For each measured frequency, a set of 64 frequencies was generated consistent with the uncertainty in the frequency. For the determination of (9), the median value of ρ_{m} was used for each data point with a weight equal to the inverse difference between the first and third quartile. Comparing (9) to (7), we see that term by term, increased ρ_{m} correlates with decreased α.

To see how well we can predict α using ρ_{m} alone, we now calculate the log average of ρ_{m} in the 64 3D bins (divided using ranges of MLT, F10.7, and AE as before). For these 64 bins, we model α with a simple formula suggested by Eureqa Formulize as

$$\alpha_{\rho_{\mathrm{m}}} = 3.3 - 2.87 \log_{10}(\rho_{\mathrm{m}}). \tag{10}$$

Here we used weights equal to the inverse of the uncertainty in the mean value of $\log_{10}(\rho_{\mathrm{m}})$. The weighted standard deviation of $\alpha_{\rho_{\mathrm{m}}}$ from $\alpha_{\mathrm{original}}$ was 0.7, significantly lower than 1.0, the standard deviation of $\alpha_{\mathrm{original}}$ with respect to its mean value, but significantly larger than 0.3, the standard difference between $\alpha_{\mathrm{3Dmodel}}$ and $\alpha_{\mathrm{original}}$. To put it another way, the mass density dependence in (10) accounts for about half the reduction in variance (proportional to the standard deviation squared) going from a mean value to $\alpha_{\mathrm{3Dmodel}}$.

Figure 8 shows the adjusted α values, $\alpha_{\mathrm{adjusted}}$, and $\alpha_{\rho_{\mathrm{m}}}$ values (also adjusted) in the same format as Figure 7. Figure 8b shows some of the same trends as Figure 8a, but the agreement with $\alpha_{\rho_{\mathrm{m}}}$ is worse than that of $\alpha_{\mathrm{3Dmodel}}$ in Figure 7b.

Takahashi et al. [2004] found evidence for α varying with the electron density n_{e}. For high n_{e} ("plasmasphere") plasma, they showed that the harmonic frequencies were consistent with a monotonic ρ_{m} dependence. The dependence for the low n_{e} ("plasmatrough") plasma was probably not consistent with a monotonic dependence. But using the power law form, as we do in this paper, the best fitting α value appeared to be more negative for low n_{e}. On the face of it, this dependence appears to be the opposite of what we find in (10), which indicates that α decreases with respect to ρ_{m}. However, we must keep in mind that the CRRES data used by Takahashi et al. were measured at solar maximum. And at solar maximum, there is a large contribution from O+ to the mass density in the plasmatrough [*Denton et al.*, 2011]. Thus during solar maximum, there may be no good

correlation between n_e and ρ_m. We are unable to explore the relation between α and n_e using data from GOES, since GOES did not measure n_e.

Despite our lack of complete theoretical understanding, we have found an empirical model for α, equation (7), that well fits the observations, at least in an average sense. This should be useful for future calculations of the frequency and field line structure of toroidal Alfvén waves and for modeling other MHD wave phenomena.

Acknowledgments. Work at Dartmouth was supported by NSF grant AGS-1105790 and NASA grants NNX10AQ60G and NNG05GJ70G. Work at JHU APL was supported by NSF Grant AGS-1106427. Values of AE come originally from the World Data Center for Geomagnetism at Kyoto University, and values of F10.7 come originally from NOAA's National Geophysical Data Center. Numerical data shown in this paper is available from the lead author upon request.

References

Angerami, J. J., and D. Carpenter (1966), Whistler studies of the plasmapause in the magnetosphere. 2. Electron density and total tube electron content near the knee in magnetospheric ionization, *Journal of Geophysical Research*, *71*(3), 711.

Chappell, C. R., M. M. Huddleston, T. E. Moore, B. L. Giles, and D. C. Delcourt (2008), Observations of the warm plasma cloak and an explanation of its formation in the magnetosphere, *J. Geophys. Res.*, *113*(A9), a09206, doi:10.1029/2007ja012945.

Denton, M. H., J. E. Borovsky, R. M. Skoug, M. F. Thomsen, B. Lavraud, M. G. Henderson, R. L. McPherron, J. C. Zhang, and M. W. Liemohn (2006a), Geomagnetic storms driven by ICME- and CIR-dominated solar wind, *J. Geophys. Res.*, *111*(A7),

doi:10.1029/2005JA011436.

Denton, R. E. (2006), Magneto-seismology using spacecraft observations, in *Magnetospheric ULF waves: Synthesis and new directions*, edited by K. Takahashi, P. J. Chi, R. E. Denton, and R. L. Lysak, Geophysical monograph, pp. 307–317, American Geophysical Union, Washington, DC, english.

Denton, R. E., and D. L. Gallagher (2000), Determining the mass density along magnetic field lines from toroidal eigenfrequencies, *J. Geophys. Res.*, *105*(A12), 27,717–27,725.

Denton, R. E., M. R. Lessard, R. Anderson, E. G. Miftakhova, and J. W. Hughes (2001), Determining the mass density along magnetic field lines from toroidal eigenfrequencies: Polynomial expansion applied to CRRES data, *J. Geophys. Res.*, *106*(A12).

Denton, R. E., K. Takahashi, R. R. Anderson, and M. P. Wuest (2004), Magnetospheric toroidal Alfvén wave harmonics and the field line distribution of mass density, *J. Geophys. Res.*, *109*(A6), A06202, doi:10.1029/2003JA010201.

Denton, R. E., K. Takahashi, I. A. Galkin, P. A. Nsumei, X. Huang, B. W. Reinisch, R. R. Anderson, M. K. Sleeper, and W. J. Hughes (2006b), Distribution of density along magnetospheric field lines, *J. Geophys. Res.*, *111*(A4), A04213, doi:10.1029/2005JA011414.

Denton, R. E., P. Decreau, M. J. Engebretson, F. Darrouzet, J. L. Posch, C. Mouikis, L. M. Kistler, C. A. Cattell, K. Takahashi, S. Schaefer, and J. Goldstein (2009), Field line distribution of density at L=4.8 inferred from observations by CLUSTER, *Ann. Geophys.*, *27*(2), 705–724.

Denton, R. E., M. F. Thomsen, K. Takahashi, R. R. Anderson, and H. J. Singer (2011), Solar cycle dependence of bulk ion composition at geosynchronous orbit, *J. Geophys. Res.*, *116*, a03212, doi:10.1029/2010ja016027.

529 Galvan, D. A., M. B. Moldwin, and B. R. Sandel (2008), Diurnal variation in plasma-
530 spheric He(+) inferred from extreme ultraviolet images, *J. Geophys. Res.*, *113*(A9),
531 a09216, doi:10.1029/2007ja013013.

532 King, J. H., and N. E. Papitashvili (2005), Solar wind spatial scales in and comparisons
533 of hourly wind and ace plasma and magnetic field data, *J. Geophys. Res.*, *110*(A2),
534 a02104, doi:10.1029/2004ja010649.

535 Kress, B. T., M. K. Hudson, M. D. Looper, J. Albert, J. G. Lyon, and C. C.
536 Goodrich (2007), Global MHD test particle simulations of >10 MeV radiation belt
537 electrons during storm sudden commencement, *J. Geophys. Res.*, pp. A09,215–1–11,
538 doi:10.1029/2006ja012218.

539 Kwon, H. J., K. H. Kim, D. H. Lee, K. Takahashi, V. Angelopoulos, E. Lee, H. Jin,
540 Y. D. Park, J. Lee, P. R. Sutcliffe, and H. U. Auster (2012), Local time-dependent Pi2
541 frequencies confirmed by simultaneous observations from THEMIS probes in the inner
542 magnetosphere and at low-latitude ground stations, *J. Geophys. Res.*, *117*, a01206,
543 doi:10.1029/2011ja016815.

544 Lee, J. H., and V. Angelopoulos (2014), On the presence and properties of cold ions
545 near earth's equatorial magnetosphere, *J. Geophys. Res.*, *119*(3), 1749–1770, doi:
546 10.1002/2013ja019305.

547 Lyons, L. (1991), *A Practical Guide to Data Analysis for Physical Science Students*, Cam-
548 bridge University Press, Cambridge.

549 McComas, D. J., S. J. Bame, B. L. Barraclough, J. R. Donart, R. C. Elphic, J. T. Gosling,
550 M. B. Moldwin, K. R. Moore, and M. F. Thomsen (1993), Magnetospheric plasma
551 analyzer - Initial 3-spacecraft observations from geosynchronous orbit, *J. Geophys. Res.*,

552 *98*(A8), 13,453–13,465.

553 Menk, F. W., D. Orr, M. A. Clilverd, A. J. Smith, C. L. Waters, D. K. Milling, and B. J.
554 Fraser (1999), Monitoring spatial and temporal variations in the dayside plasmasphere
555 using geomagnetic field line resonances, *J. Geophys. Res.*, *104*(A9), 19,955–19,969, doi:
556 10.1029/1999ja900205.

557 Perry, K. L., M. K. Hudson, and S. R. Elkington (2005), Incorporating spectral charac-
558 teristics of Pc5 waves into three- dimensional radiation belt modeling and the diffusion
559 of relativistic electrons, *J. Geophys. Res.*, *110*(A3), a03215, doi:10.1029/2004ja010760.

560 Press, W. H., B. P. Flannery, S. A. Teukolsky, and W. T. Vetterling (1986), *Numerical*
561 *Recipes*, Cambridge Univ. Press, New York.

562 Price, I. A., C. L. Waters, F. W. Menk, G. J. Bailey, and B. J. Fraser (1999), A technique to
563 investigate plasma mass density in the topside ionosphere using ULF waves, *J. Geophys.*
564 *Res.*, *104*(A6).

565 Schmidt, M., and H. Lipson (2009), Distilling free-form natural laws from experimental
566 data, *Science*, *324*(5923), 81–85, doi:10.1126/science.1165893.

567 Schulz, M. (1996), Eigenfrequencies of geomagnetic field lines and implications for plasma-
568 density modeling, *J. Geophys. Res.*, *101*(A8), 17,385–17,397, doi:10.1029/95ja03727.

569 Singer, H. J., D. J. Southwood, R. J. Walker, and M. G. Kivelson (1981), Alfven-wave
570 resonances in a realistic magnetospheric magnetic-field geometry, *J. Geophys. Res.*,
571 *86*(NA6).

572 Takahashi, K., and R. E. Denton (2007), Magnetospheric seismology using multiharmonic
573 toroidal waves observed at geosynchronous orbit, *J. Geophys. Res.*, *112*(A5), A05204,
574 doi:10.1029/2006JA011709.

Takahashi, K., and R. L. McPherron (1982), Harmonic structure of pc 3-4 pulsations, *J. Geophys. Res.*, *87*(NA3), 1504–1516.

Takahashi, K., R. E. Denton, R. R. Anderson, and W. J. Hughes (2004), Frequencies of standing Alfven wave harmonics and their implication for plasma mass distribution along geomagnetic field lines: Statistical analysis of CRRES data, *J. Geophys. Res.*, *109*(A8), A08202, doi:10.1029/2003JA010345.

Takahashi, K., R. E. Denton, and H. J. Singer (2010), Solar cycle variation of geosynchronous plasma mass density derived from the frequency of standing alfven waves, *J. Geophys. Res.*, *115*, doi:10.1029/2009ja015243.

Takahashi, K., R. E. Denton, W. Kurth, C. Kletzing, J. Wygant, J. Bonnell, L. Dai, K. Min, C. W. Smith, and R. MacDowall (2014), Externally driven plasmaspheric ULF waves observed by the Van Allen Probes, *J. Geophys. Res.*, *119*.

Tsyganenko, N. A., and M. I. Sitnov (2005), Modeling the dynamics of the inner magnetosphere during strong geomagnetic storms, *J. Geophys. Res.*, *110*(A3), doi:10.1029/2004ja010798.

Waters, C. L., F. W. Menk, M. F. Thomsen, C. Foster, and F. R. Fenrich (2006), Remote-sensing the magnetosphere using ground-based observations of ULF waves, in *Magnetospheric ULF Waves: Synthesis and New Directions*, edited by K. Takahashi, P. J. Chi, R. E. Denton, and R. L. Lysak, Geophysical Monograph, pp. 319–340, American Geophysical Union, Washington D.C.

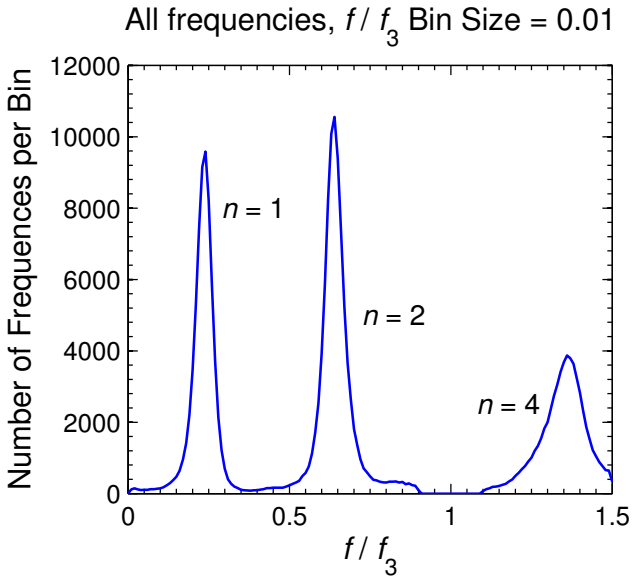

Figure 1. Distribution of normalized frequencies $\bar{f} \equiv f/f_3$ for the entire data set used in this paper. The bin size for $\bar{f}$ is 0.01.

Table 1. Minimum, 8 Bin Quantile Divisions Q_i, and Maximum Values for Parameters MLT, F10.7, and AE

Parameter	Min	Q_1	$\mathbf{Q_2}$[a]	Q_3	$\mathbf{Q_4}$[a]	Q_5	$\mathbf{Q_6}$[a]	Q_7	Max
MLT (h)	0.01	5.39	**6.69**	7.80	**8.93**	10.22	**11.91**	14.20	23.99
F10.7 (sfu)	65.9	70.1	**73.7**	80.5	**94.4**	115.8	**144.6**	184.7	346.5
AE (nT)	10.2	58.6	**88.2**	126.8	**175.1**	234.6	**315.8**	446.8	1794.

[a] The boldface Q_i values are used in section 4 to divide the data into four bins.

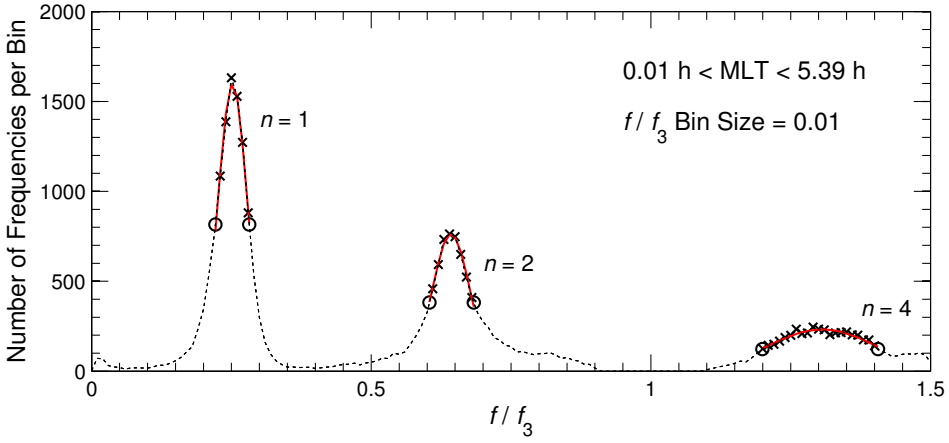

Figure 2. Distribution of frequencies $\bar{f}$ in the three peaks (black x symbols) for the 1D bin with the lowest values of MLT (0.01 h $\leq$ MLT $<$ 5.39 h). The red curves are Gaussian fits to the peaks.

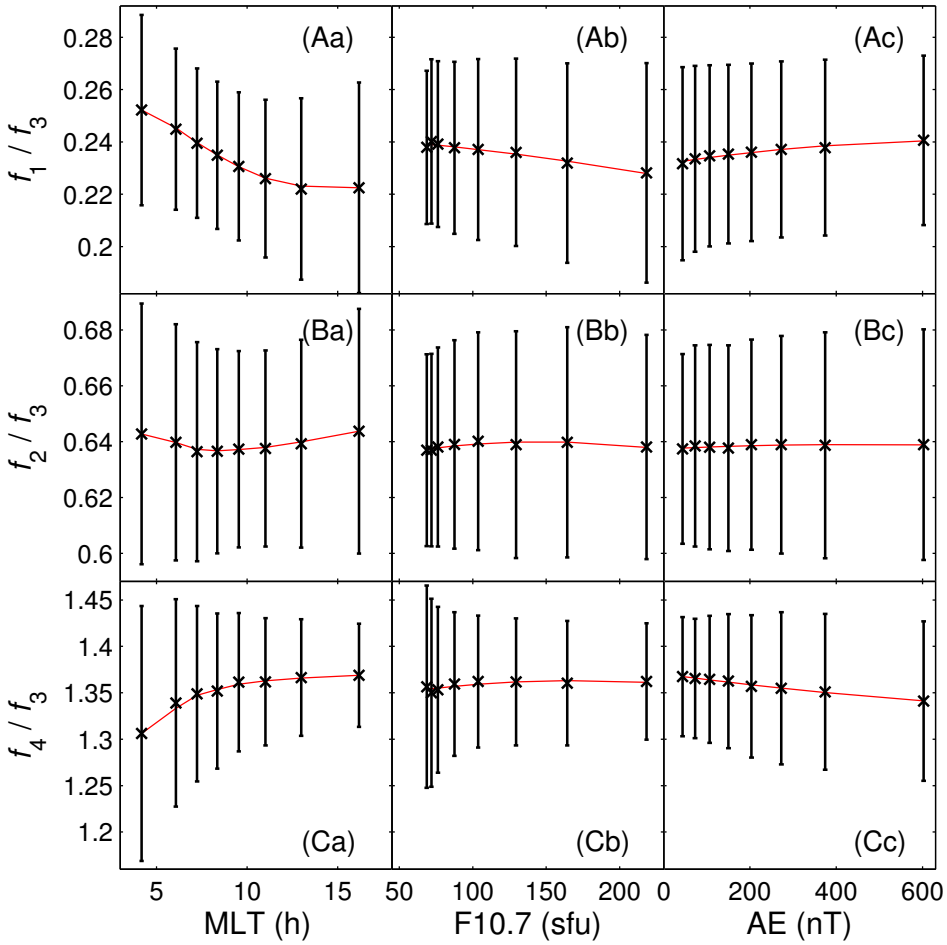

Figure 3. Peak normalized frequency $\bar{f}_n \equiv f_n/f_3$ for $n = 1$ (row A), $n = 2$ (row B), and $n = 4$ (row C) versus MLT (column a), F10.7 (column b), and AE (column c). The values from the fits in each bin are the black x symbols and the red curves are the values smoothed as described in the text.

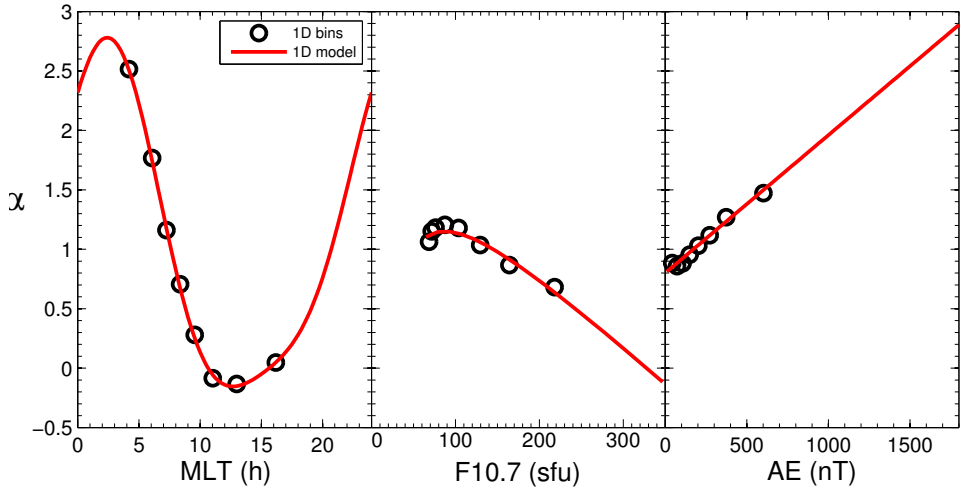

Figure 4. Values of the power law coefficient α versus (a) MLT, (b) F10.7, and (c) AE. The black circles are the values of α calculated using the 1D binned frequency ratios in Figure 3. The red curves are the analytical models (4–6) described in the text.

Table 2. Mean Values of Parameters MLT, F10.7, and AE, in 4 Bins Divided Using the Individual Parameters

Parameter	Bin 1	Bin 2	Bin 3	Bin 4
MLT (h)	5.1	7.8	10.3	14.6
F10.7 (sfu)	70.	82.	117.	191.
AE (nT)	58.	128.	238.	488.

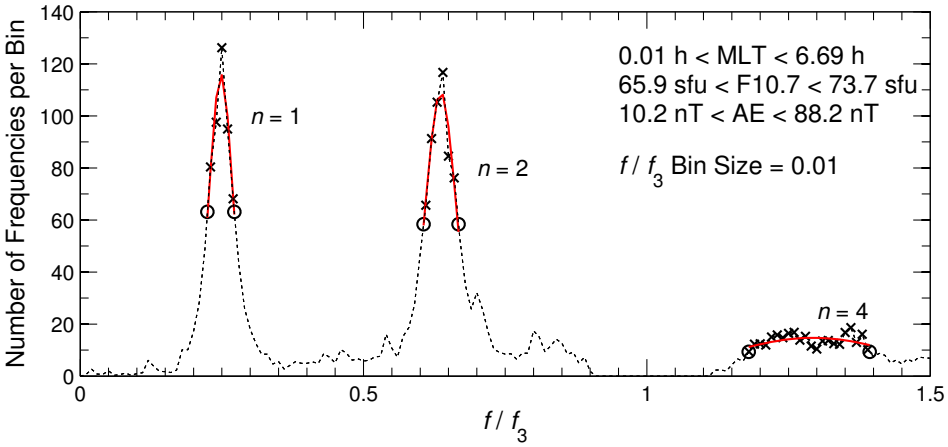

Figure 5. Like Figure 2, but for the 3D bin with the lowest values of MLT, F10.7, and AE. The ranges are listed in the panel.

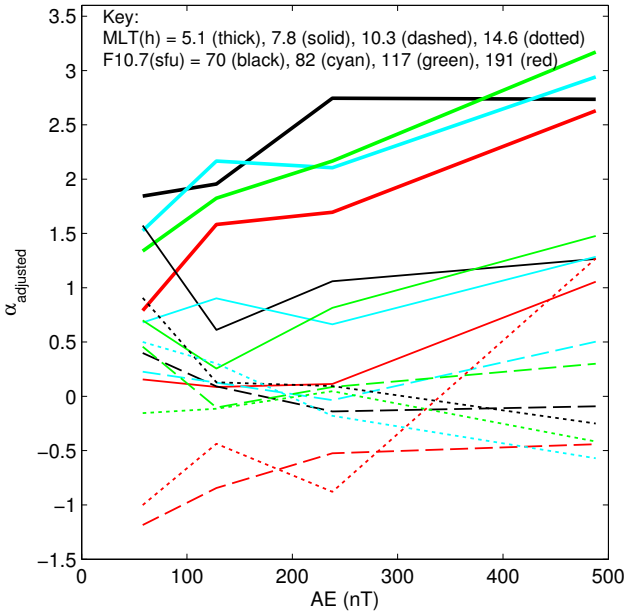

Figure 6. Values of $\alpha_{adjusted}$ versus AE for the 3D data. The curves vary in color corresponding to F10.7 values, and they vary in line style corresponding to MLT values, as indicated in the key. Higher F10.7 values are indicated by colors that are more red, and higher MLT values are indicated by line styles that are less weighty in appearance. (The thin dotted curve is the least weighty, while the thick solid curve is the most weighty.) In the key, "thick" indicates the thick solid curves, and "solid" indicates the thin solid curves.

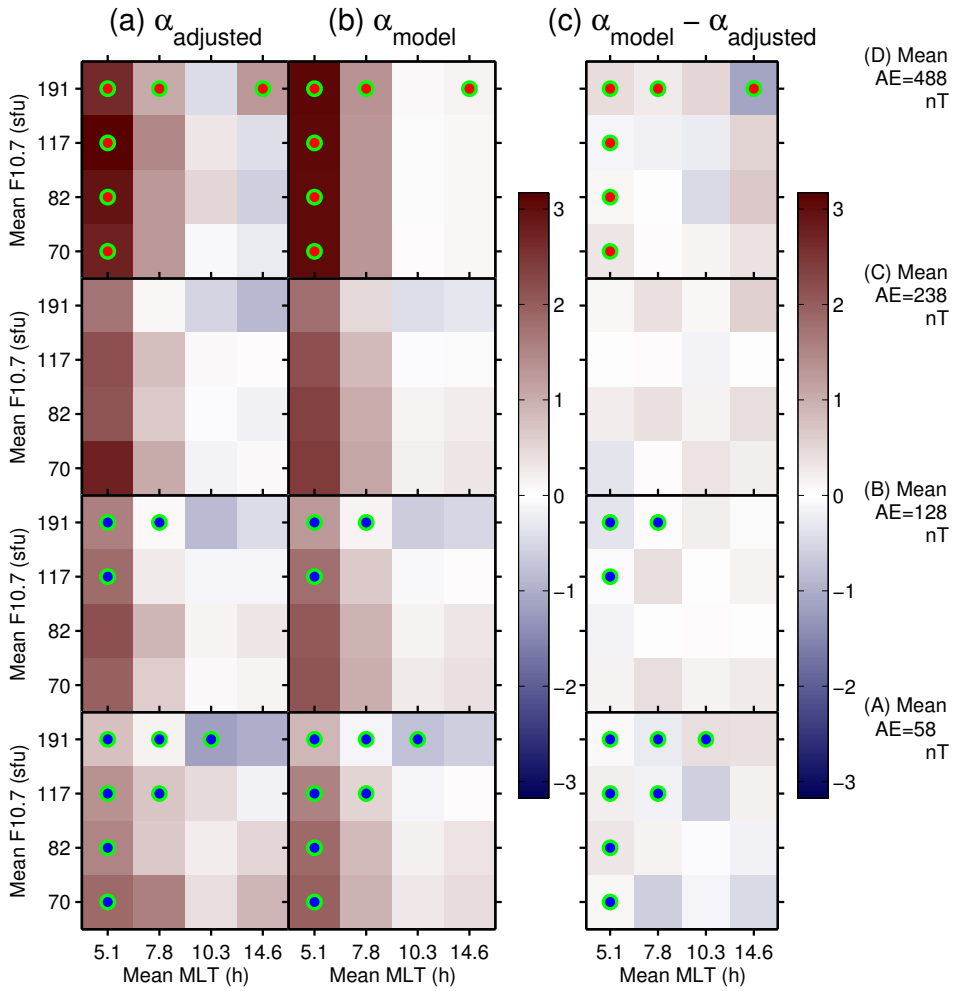

Figure 7. (a) Adjusted α values, α_{adjusted}, in the 3D bins, (b) model values, α_{model}, found using (7), and (c) $\alpha_{\text{model}} - \alpha_{\text{adjusted}}$, for (A) AE = 58 (bottom row or panels), (B) AE = 128, (C) AE = 238, and (D) AE = 488. In each panel, the values of α are shown using the blue to red color scale (at right) versus MLT on the horizontal axis and F10.7 on the vertical axis. The green circles (some of which may appear to be cyan) are points where the AE dependence led to a change in α_{model} of at least 0.4 as described in the text.

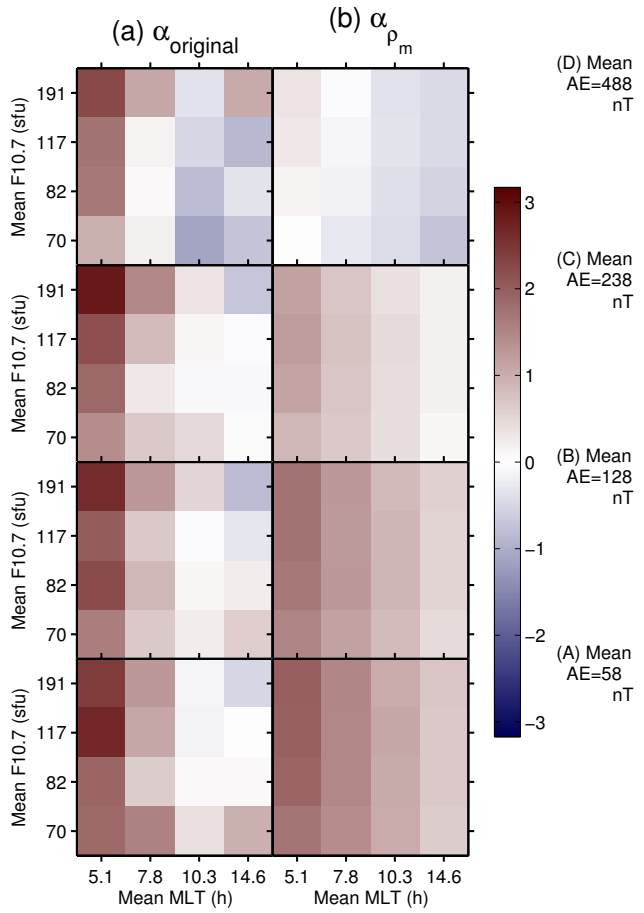

Figure 8. (a) Adjusted α values, α_{adjusted}, in the 3D bins, and (b) model values $\alpha_{\rho_{\text{m}}}$ using (10), for (A) AE = 58 (bottom row of panels), (B) AE = 128, (C) AE = 238, and (D) AE = 488. In each panel, the values of α are shown using the blue to red color scale (at right) versus MLT on the horizontal axis and F10.7 on the vertical axis.